Water Practice & Technology

IWA PUBLISHING

Water Practice & Technology Vol 19 No 4, 1219 doi: 10.2166/wpt.2024.042

Green synthesis of zinc oxide nanoparticles from *Salvadora persica* leaf extract: Characterization and studying methyl orange removal by adsorption

Amal S. Al Rahbi[a,*], Ahlam H. Al Mawali[a], Shahad S. Al Rawahi[a], Rima K. Al Dighishi[a], Fatma A. Al Abri[a], Anwar Ahmed[b] and Sadik Rahman[c]

[a] Department of Applied Sciences, College of Applied Sciences and Pharmacy, University of Technology and Applied Sciences, Muscat, PO 74 Postal code 133, Oman
[b] Civil and Environmental Engineering Department, College of Engineering and Architecture, University of Nizwa, Nizwa, PO 33 Postal code 616, Oman
[c] Department of Civil Engineering, East West University, Jahurul Islam Ave, Dhaka 1212, Bangladesh
*Corresponding author. E-mail: amal.alrahbi@utas.edu.om

ABSTRACT

The present study conducted a successful green synthesis of zinc oxide nanoparticles (ZnO NPs) from the aqueous solution of *Salvadora persica* leaf extract as capping agent and used for methyl orange dye removal. The morphology, chemical composition, crystallinity, optical property and isothermal behavior of synthesized nanoparticles were characterized by scanning electron microscopy (SEM), energy dispersive spectroscopy (EDX), Fourier transform infra-red (FTIR), X-ray diffraction (XRD), and UV-visible spectroscopy (UV-Vis). The influencing factors on MO removal such as preparation method, dose, pH, contact time, and dye concentration were examined. The UV-Vis absorption band was found at 365 nm and the XRD analysis confirmed the crystallinity of the ZnO NP and the particle sizes were in the range of 32-68 nm. The FTIR bands confirm the presence of bioactive compounds. SEM images showed the formation of hexagonal and rod-shaped nanoparticles. The results revealed that a maximum methyl orange removal of 68% was obtained with an amount of 0.05 g of ZnO NPs at pH 5. The adsorption process can be well explained by the Langmuir isotherm model. This research demonstrates a green method of preparing various ZnO nanoparticle with a remarkable efficiency towards the removal of methyl orange dye.

Key words: green synthesis, hexagonal, nanorods, wastewater, ZnO nanoparticles

HIGHLIGHT

- This study describes, for the first time, a facile green approach for the synthesis of ZnO nanoparticles using an aqueous leaf extract of *Salvadora persica* for methyl orange removal.

GRAPHICAL ABSTRACT

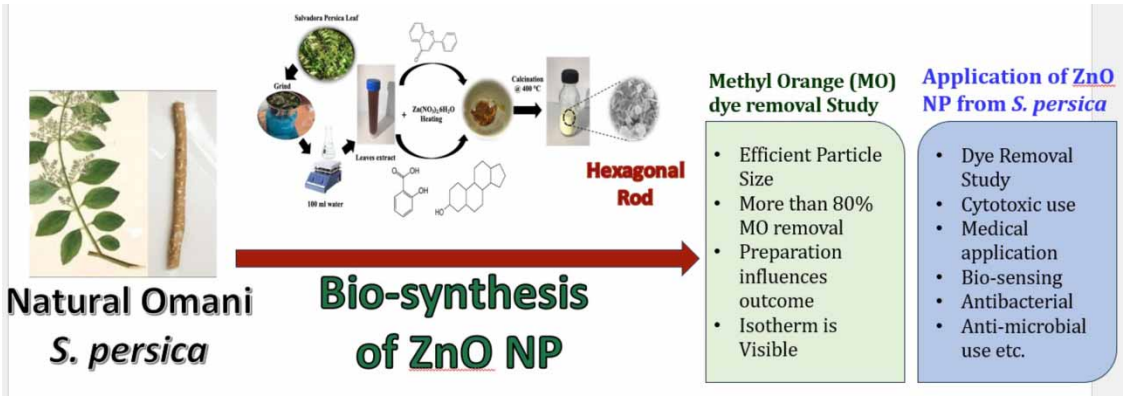

1. INTRODUCTION

Zinc oxide (ZnO) is a versatile metal oxide with various desirable properties. ZnO is safe, and biocompatible with unique properties like optical, electrical, semiconducting, and chemical sensing. ZnO nanoparticles (NPs) are being

used as promising nanomaterials as cosmetic additives, antibacterial, additives, chemical absorbents, catalysts, and polymer additives because of their long life span, specific surface area, and high pore volume. Due to these properties, it has been used in various industrial applications, such as solar cells, pharmaceuticals, cosmetics, photocatalysts, and gas sensors (Yang & Park 2008; Khorsand Zak *et al.* 2011; Salahuddin *et al.* 2015; Modi *et al.* 2022).

Different methods are currently used to synthesize ZnO NPs including sol-gel, thermal decomposition, solvothermal, chemical vapour synthesis, laser ablation, and precipitation strategies (Yedurkar *et al.* 2016). These methods are labour intensive, costly, and potentially harmful to living organisms and the environment. Consequently, the development of cost-effective and green synthesis methods received high attention from material scientists in the field of biotechnology due to low cost, environmental friendly nature, simplicity of implementation, and dependability. The green synthesis technique does not employ toxic chemicals but rather uses natural and easy-to-get resources such as enzymes, microorganisms, and plant extracts (Basnet *et al.* 2018). The facile green synthesis method is stable and produces metal NPs with well-defined sizes and shapes from their metallic salts. However, NP activity might be affected by shape, size, and surface chemistry. Many biological organisms including plants (Suresh *et al.* 2018; Iqbal *et al.* 2022; Modi *et al.* 2022; Pathania *et al.* 2022; Sharma *et al.* 2022), bacteria (Lengke *et al.* 2007), yeast (Kowshik *et al.* 2002), and fungus (Rautaray *et al.* 2003) have been demonstrated to have the ability to use reductive properties of their proteins and metabolites to transform inorganic metal ions into metal NPs. The capability of green synthesis and capping has been demonstrated in extensive research with plants from many taxonomic groups (Rautaray *et al.* 2003; Joglekar *et al.* 2011; Das *et al.* 2013; El-Rafie *et al.* 2013). Plant extracts have phytochemicals such as alkaloids, flavonoids, amino acids, alkaloids, vitamins, and alcohol that act as stabilizing and reducing agents for metal ions (Nava *et al.* 2017). These reductive agents can react with zinc salts to form ZnO NPs using different capping agents (Xu *et al.* 2021). Several researchers have synthesized ZnO NPs from plant extracts like *Moringa oleifera* extract (Matinise *et al.* 2017), *Brassica oleracea L. var. italica* extract (Sendal *et al.* 2022), peeled extract of *Nephelium lappaceum L.* (Karnan & Selvakumar 2016), etc.

Rapid industrialization and urbanization have resulted in the discharge of many chemical contaminants such as heavy metals and dyes into natural water bodies (Garg *et al.* 2020). Water pollution is considered a global issue, and various treatment methods have been developed. Dyes are the most extensive source of colour in leather goods, footwear, paper, pharmaceuticals, clothing, food, printing industries, etc. (Pathania *et al.* 2022). The presence of dyes in water has a negative influence on various aquatic organisms because they can generate cancer and mutagens (Mezohegyi *et al.* 2012). Azo dyes and inks account for more than half of the dyes and inks used in the textile industry owing to their colour range and low cost. Methyl orange (MO) is an azo-derived chemical compound with weak acidic properties and the potential to function as a carcinogenic agent (Vargas *et al.* 2021). Therefore, the removal of MO dye was investigated by various methods (Peerakiatkhajohn *et al.* 2021). However, successful methods or combinations of processes are yet to be explored, which can be inexpensive and environment friendly for complete removal.

This study describes, for the first time, a facile green approach for the synthesis of ZnO NPs using an aqueous leaf extract of *Salvadora persica* for MO removal. *Salvadora* is a large evergreen tree that is found in arid coastal areas, desert flood plains, and saline areas (Haque & Alsareii 2015). Traditionally, the plant is used for various purposes, including food, oral hygiene, fuel, cosmetics, and medications. Reuben *et al.* (2011) performed a phytochemical screening of the aqueous extract of *S. persica* leaves and showed the presence of flavonoids, sterols, saponins, tannins, and flavone aglycones (Reuben *et al.* 2011). These phytochemicals can be used as precursor agents to extract desired NPs (like silver NPs, Ag-doped ZnO NPs, silver nickel NPs, etc.), which have been reported in various studies. Few studies also reported the biosynthesis of ZnO NPs from *S. persica*. Those studies used *S. persica* root and leaf extract to synthesize ZnO NP for characterization and applications like cytotoxic activity, methylene blue dye removal, etc. (Miri & Sarani 2019; Verma *et al.* 2020). However, the precursors were different in those studies, which made morphologically different NPs of ZnO. Information on the contributing factors of dye removal is also rarely investigated. Very few studies are available on using *S. persica* leaf extract for the green synthesis of ZnO NPs; however, the removal of an important azo dye, i.e. MO removal by adsorption, and studying its operating factors are yet explored. Therefore, this study aimed to investigate ZnO NP preparation via green synthesis using *S. persica* leaves for MO removal by adsorption. After the synthesis, the optical and structural properties were analysed by UV-vis spectra, X-ray diffraction (XRD), and Fourier transform infrared (FTIR). Morphological and elemental properties were carried out by Field emission scanning electron microscopy-energy dispersive spectroscopy (FESEM-EDX). The removal study of MO was analysed by UV-vis spectroscopy on various operating factors like solution pH, adsorbent dose, the influence of contact time, and

the initial dye concentration on dye removal. Finally, the adsorption isotherm of MO removal was analysed for the newly synthesized ZnO NPs.

2. MATERIALS AND METHODS

2.1. Materials

Zinc nitrate hexahydrate $Zn(NO_3)_2.6H_2O$ and pure MO ($C_{14}H_{14}N_3NaO_3S$) dye powders were supplied by Sigma-Aldrich and used as received. Fresh leaves of *S. persica* were collected from a local farm in Barka, Oman. All analytical grade chemicals were used as received.

2.2. Preparation of *Salvadora* leaf extract

The collected *S. persica* (SP) leaves were washed thoroughly with distilled water and dried under sunlight. The dried leaves were ground to powder using a grinder. *S. persica* leaves were then used to make boiled (SP) and unboiled leaf extracts (SU). To prepare boiled leaf extracts, distilled water was added to 3 and 9 g of SP powder and then boiled at 60 °C for 1 h with stirring. The plant extracts were cooled to room temperature and then filtered to obtain the clear extract. The synthesized NPs using 3 and 9 g of SP were labelled as ZnO-SP1 and ZnO-SP2, respectively. The unboiled leaf extract (labelled as ZnO-SU) was prepared using the same procedure but without heating.

2.3. Green synthesis of ZnO NPs

Green synthesis of ZnO NPs (Figure 1) was carried out according to the method reported by Khan *et al.* (2019) with some modifications. A 30 ml of the prepared plant extracts was placed in different beakers and heated up to 60 °C. Next, 3 g of $Zn(NO_3)_2.6H_2O$ was added to each beaker and kept on a magnetic stirrer. The reaction was conducted for 3 h until a yellow paste was obtained. The formed paste was then calcined at 400 °C for 2 h to obtain a yellowish-white powder of ZnO. The annealed powder was used for further characterization. The synthesized NPs using 3 and 9 g of SP were labelled as ZnO-SP1 and ZnO-SP2, respectively. The NPs synthesized with unboiled leaf extract were labelled as ZnO-SU.

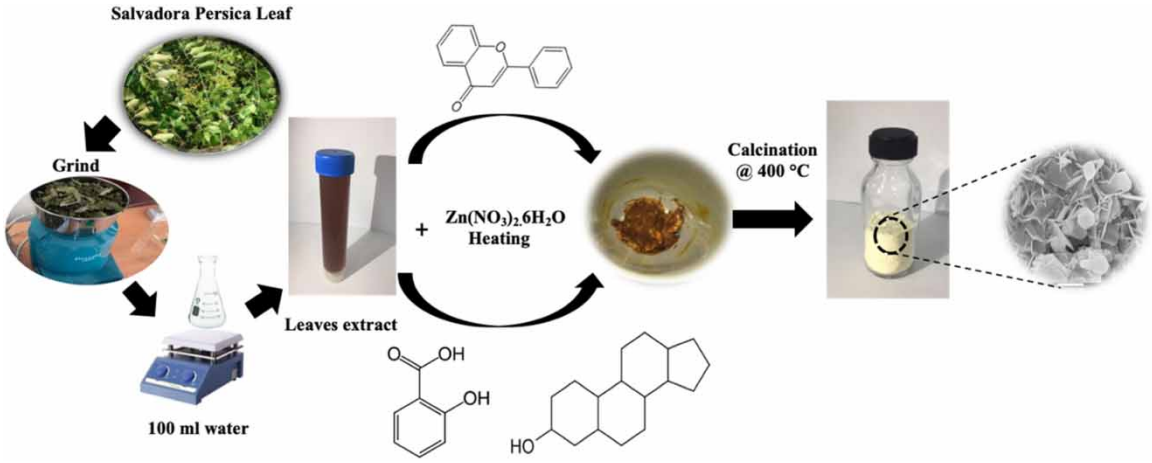

Figure 1 | Process of synthesis of zinc oxide nanoparticles.

2.4. Material characterization

Preliminary detection of the synthesized NPs was achieved through a visual colour change. Several analytical techniques have been employed to characterize the green-synthesized ZnO NPs. The optical properties of the prepared NPs were monitored by UV-Vis spectral analysis in the range between 200 and 700 nm using a UV-Vis spectrophotometer (Evolution 300-Thermo Fisher Scientific). FTIR spectra were obtained using FTIR spectrophotometer (Shimadzu spectrophotometer (Kyoto, Japan) in the 500–4000 cm^{-1} region. Patterns of XRD were obtained for the synthesized NPs using an XRD apparatus (PANalytical, XPert PRO, USA) over the range of $2\theta = 20–70°$ and with Cu-Kα ($\lambda = 0.15406$ nm) radiation. Elemental analysis was performed using an EDX. The shape and surface morphology of the prepared NPs were determined by field emission scanning electron microscopy (SEM; JSM-7600F-JEOL).

2.5. MO removal

The ability of the synthesized ZnO NPs to remove dyes was examined using MO as the model dye. UV-Vis spectra were collected from aliquots of solutions containing 5–20 ppm MO concentrations, and the maximum absorbance values were located at 460 nm (Figure 2(a)). The calibration curve for the water–MO system was first obtained to evaluate MO degradation (Figure 2(b)).

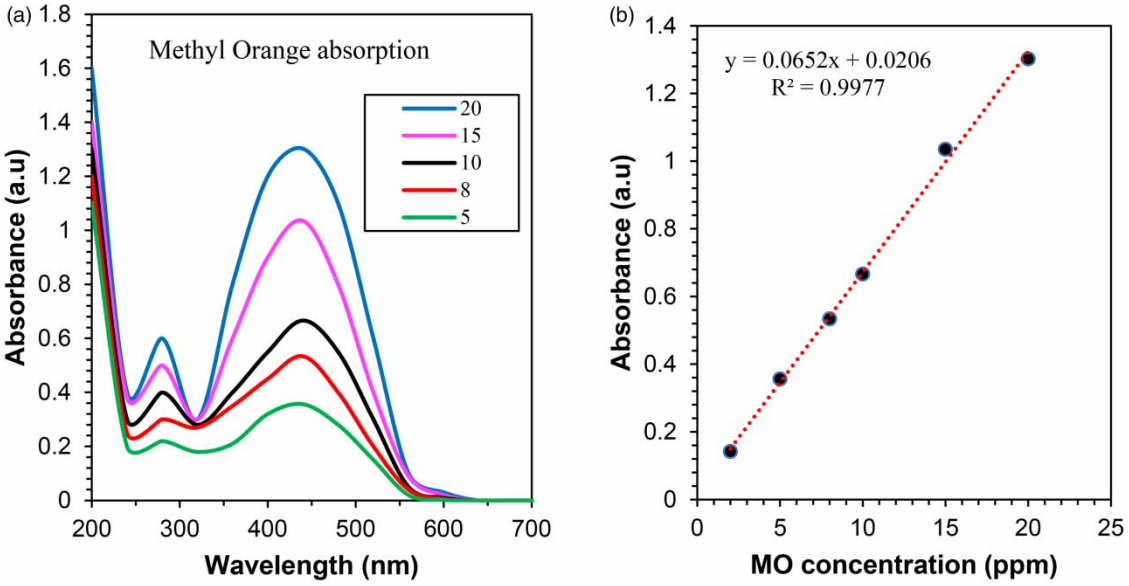

Figure 2 | (a) UV-vis absorption spectra corresponding to different concentrations of methyl orange and (b) calibration curve to determine the amount of MO present in a solution at maximum peak absorbance (~460 nm).

To evaluate the effectiveness of the synthesized ZnO NPs to remove MO, about 20 mg of the synthesized NPs was dispersed in 10 ml of 10 ppm of MO solution at room temperature and with a constant stirring for 30 min to ensure good particle dispersion in the solution. To study the influence of the pH of the solution on MO removal, experiments at various initial pH ranges of 1–7 were conducted for an initial dye concentration of 10 ppm. The influence of the adsorbent amount on dye removal was investigated by varying the NP dose from 0.01 to 0.05 g. To observe the effect of duration time on dye removal, the contact time was varied from 20 to 100 min. In addition, the influence of dye concentration was examined by varying the dye concentration from 5 to 20 mg/l, and the other experimental parameters were kept constant.

The dye concentration of the aqueous solution was measured before and after the experiment using a UV-Vis spectrophotometer at 460 nm. A common adsorbent dose of 0.02 g, contact time of 30 min, concentration of 10 ppm and pH of 5 were used for all experiments. The percentage dye removal efficiency (R%) and the amount adsorbed per adsorbent unit weight (q_e) were calculated as follows:

$$\text{Removal } (\%) = \frac{C_i - C_e}{C_e} \times 100 \tag{1}$$

$$q_e = \frac{(C_i - C_e)V}{M} \tag{2}$$

where C_i and C_e are the initial and final dye concentrations (mg/L), respectively; V denotes the volume of solution (L); and M represents the mass of adsorbent (g).

3. RESULTS AND DISCUSSION

3.1. Optical and structural properties

ZnO NPs were obtained using fresh leaf extract of *S. persica,* which contains stabilizing and reducing agents such as terpenoids and flavonoids (Aumeeruddy *et al.* 2018). The formation of ZnO NPs was confirmed by the visual examination. The addition of $Zn(NO_3)_2.6H_2O$ to the leaf mixture has changed the colour to yellow, indicating the

formation of ZnO NPs. After calcination, a yellowish-white powder was formed (Figure 1). This observation agreed with the results obtained by Khan *et al.* (2019).

The distinctive optical characteristics of NPs are caused by surface plasmon resonance, which depends mainly on their size and shape. The absorption spectra of the synthesized ZnO NPs are presented in Figure 3(a). The surface plasmon resonance band generally increased with the increase in plant concentration. From the obtained spectra, SB1 and SB2 showed absorbance at 365 and 368 nm, respectively. The absorbance slightly increases up to a wavelength of 371 for ZnO prepared from unboiled extract, confirming the successful green synthesis of ZnO NPs. According to the reported studies, the absorbance of the green-synthesized ZnO was obtained at the wavelength of 374 nm in the study by Selim *et al.* (2020) and 374 nm in the study by Patil & Taranath (2018). The shift of the absorption peak towards the higher wavelength region with the increasing concentration is attributed to the variation in particle size. According to Gupta *et al.* (2015), the absorption edge shifted to a higher wavelength with increasing NP sizes (Gupta *et al.* 2015).

The green-synthesized zinc NPs were analysed using FTIR to detect the phytochemicals that are stabilizing and capping the NPs. The FTIR spectra of the plant and synthesized ZnO NPs are presented in Figure 3(b). The highly intense peak located at 3,000–3,500 cm^{-1} denoted the presence of -OH groups. The peaks located at 2917.17,

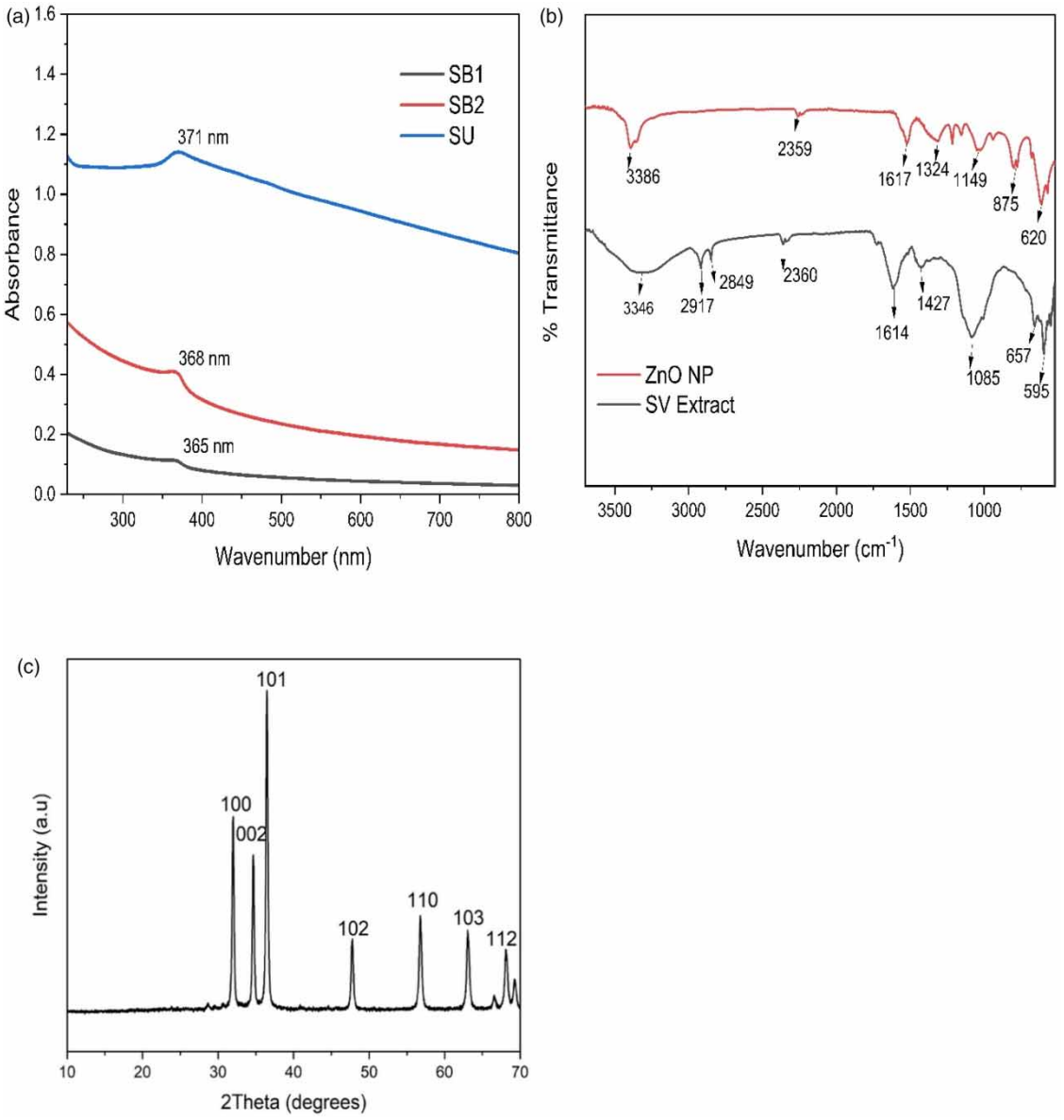

Figure 3 | (a) Ultraviolet spectra, (b) Fourier transform infrared, and (c) X-ray diffraction of the synthesized ZnO NPs.

2849.13, and 2360.25 cm^{-1} were attributed to the C = C alkyne stretching. The bands observed at 1,614, 1,427, and 1,085 cm^{-1} were assigned to C = O stretching in polyphenols, C-N stretch in primary amines, and C-O stretching in amino acids, respectively (Alharthi *et al.* 2020).

The interaction of the functional groups with the ZnO NPs was identified as the cause of a slight change and shift in the position and intensity of some associated peaks in the produced nanoparticles' FTIR spectra. The extract's primary biomolecules were bound or capped to the ZnO NPs' surface (Alamdari *et al.* 2020). The obtained results confirmed the contribution of phenols, polyphenols, and primary amines in capping and stabilizing the formed ZnO NPs. The spectra shown in Figure 3(b) reveal the presence of a new band at 875 cm^{-1}, which was assigned to the ZnO stretching band (Jan *et al.* 2020). The FTIR spectra confirmed the successful capping of biomolecules on the synthesized NPs.

The size and crystalline nature of ZnO NPs were determined using XRD analysis. The XRD pattern provided peaks at 2θ from 0 to 70° in which the highest relative intensities of the ZnO NPs were observed at $2\theta = 31.61$, 34.28, 36.12, 47.39, 56.42, 62.69, and 68.90°. The sharp peaks are related to the (100), (002), (101), (102), (110), (103), and (112) crystallographic phase of a hexagonal wurtzite structure of zinc oxide (Kahsay *et al.* 2019). Similar patterns were reported using the leaf extracts of *S. persica* (Alharthi *et al.* 2020), *Euphorbia sanguinea* (Ekennia *et al.* 2021), and *Costus woodsonii* (Khan *et al.* 2019). The hexagonal wurtzite structure is more stable under ambient conditions than the cubic zinc blend. The XRD pattern contained only zinc oxide peaks, which confirms the purity of the synthesized ZnO NPs.

3.2. Compositional and morphological properties

SEM-EDX analysis was used to assess the surface morphology and the elemental content of the produced ZnO NPs, and the obtained results are presented in Figure 4. Figure 4 clearly shows the formation of hexagonal and rod-shaped ZnO NPs. This rod-shaped ZnO NP formation is matched with a previous study where ZnO was synthesized using *S. persica* leaf extract (Alharthi *et al.* 2020). It is also agreed with those obtained by Suresh *et al.* (2018) where ZnO NPs with hexagonal and rod shapes were formed from green synthesis using *Costus pictus* plants.

The shape of the ZnO NPs became clear and with a well-defined shape as the amount of plant extract increased. The active components increased with the increase of plant amounts which resulted in changing the morphology of the obtained NPs. It has been reported by Andres *et al.* (1990) and Pacholski *et al.* (2002) that the precursor concentration significantly affects the shape of ZnO nanostructures. In the study by Lakshmeesha *et al.* (2014), ZnO NPs with flaky flower, rose-like, hexagonal, bud, and a bell shape microstructure were found to form with increasing the amount of *Nerium oleander* leaf extract. In addition, many factors such as heating, plant extract, and concentration have been found to influence nanorod formation. In this study, the temperature at which that plant extract was prepared was found to play a major role in determining the morphology of ZnO NPs. In this regard, at 60 °C, rod-shaped NPs were obtained (Figure 4(a) and 4(b)), and at room temperature, hexagonal particles were formed (Figure 4(c)). From the microscopic analysis, it can be concluded that the extract preparation method plays a major role in obtaining different morphologies of ZnO. Boiling *Salvadora* leaf extract yielded a mixture of hexagonal and nanorod ZnO. However, hexagonal ZnO NPs were formed when *Salvadora* leaf extract was prepared without heating.

The EDX peaks (Figure 4) confirm the presence of zinc and oxygen, which clearly indicates the formation of ZnO NPs. The peaks showed that SB-1 had 40.8% Zn and 26.1% O_2, SB-2 had 58.2% Zn and 18.9% O_2, and SU had 62.3% Zn and 18.4% O_2. Minor elemental traces of aluminium, calcium, chloride, potassium, and magnesium, which were derived from the plant material, were also present.

3.3. Methyl orange removal by the synthesized ZnO NPs

The uptake of pollutants onto adsorbent materials is influenced by various parameters, including the concentration of the dye, the contact duration, the solution pH, temperature, and the dosage of adsorbent. The influence of some of these parameters on the MO removal by ZnO NPs was investigated. Different NP structures have different degrees of reaction sites. Sharma (2016) investigated the influence of different ZnO NP structures on Alizarin Red S dye removal (Sharma 2016). Among the studied structures, the nano-flower was found to be the most efficient photocatalyst.

To assess the influence of ZnO morphology, the influence of different shapes of ZnO NPs on dye removal was examined using a well-known model dye, MO. Figure 5(a) and 5(b) shows MO absorption spectra under UV-Vis

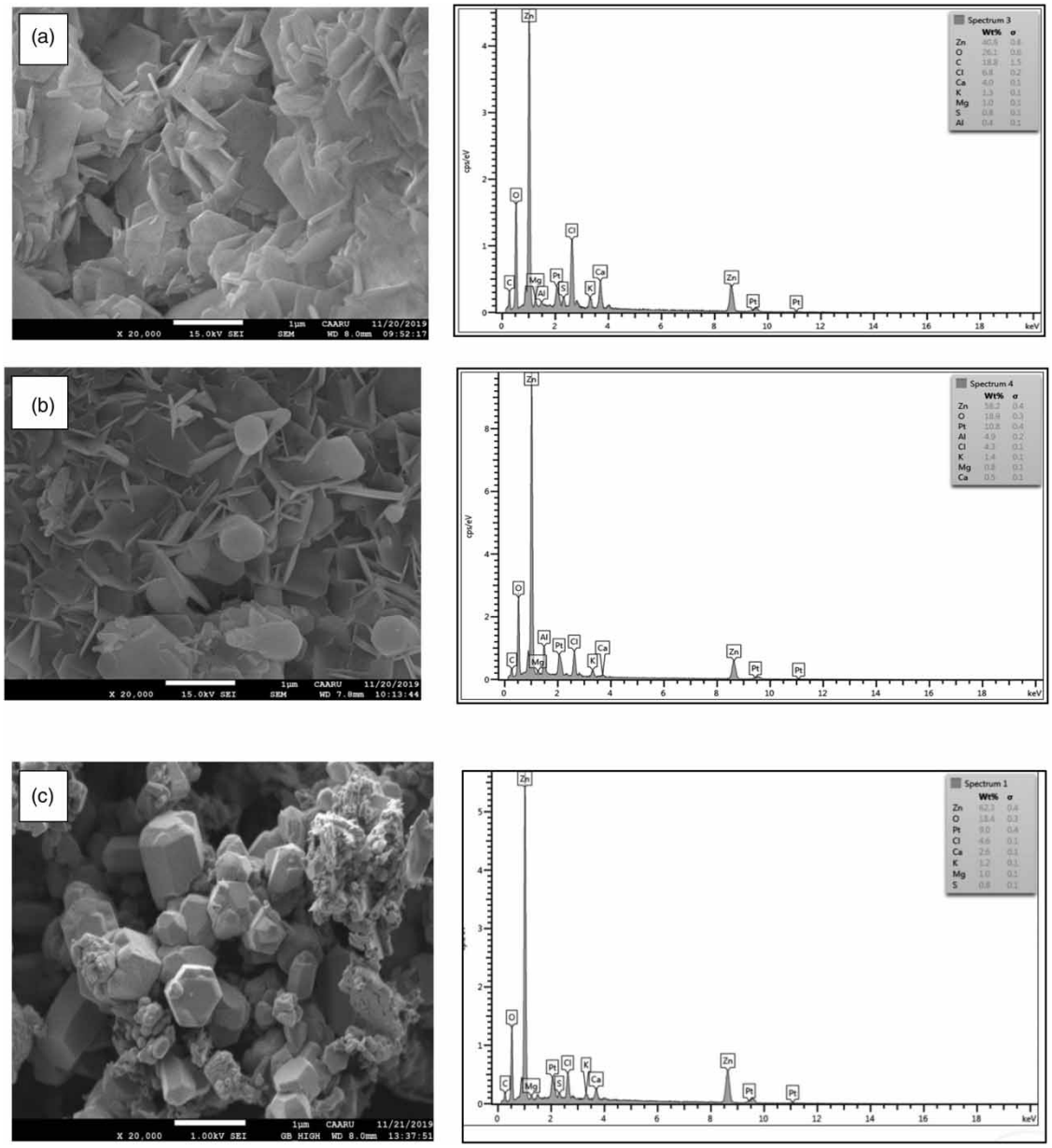

Figure 4 | SEM-EDX images of the synthesized ZnO NPs: (a) SB1, (b) SB2, and (c) SU.

light using 0.02 g of SB2 and SU ZnO NPs, respectively. The peak at 460 nm corresponded to the absorption peak of MO, which decreased rapidly with time without shifting in the absorption maximum. The superiority of SB2 can be due to the nanorods of ZnO, probably because of the high number of reaction sites. It can be concluded that dye removal is highly affected by the morphology of the NPs.

3.3.1. Influence of contact duration

Figure 6(a) shows the influence of contact time on MO removal. The result reveals a consistent rise in adsorption as the time increased from 20 to 80 min. However, beyond this point, there was no noticeable change in the MO removal by the ZnO NPs, indicating the attainment of equilibrium. This lack of change was due to the decreasing interaction between the active sites of ZnO NPs and MO molecules over time, primarily because these sites became fully occupied. The achieved equilibrium can be attributed to the saturation of the sites of ZnO NPs. SB1, SB2, and SU reached their equilibrium on MO removal at 80 min, which corresponds to 56.7, 80, and 42% removal, respectively.

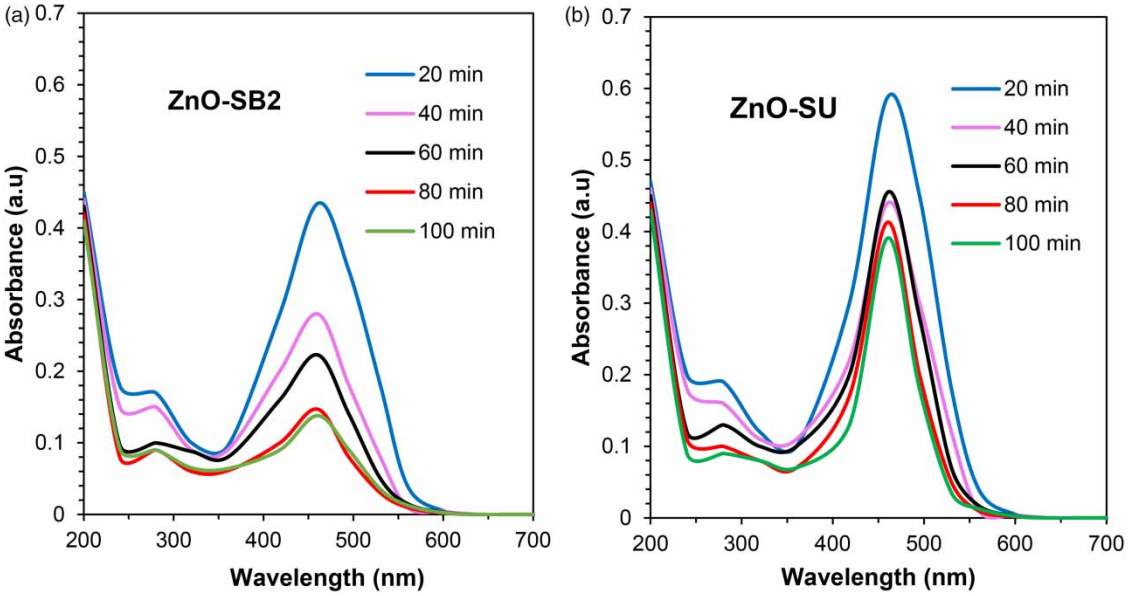

Figure 5 | Resultant spectra of UV-Vis spectroscopy using aqueous solutions of MO treated with (a) ZnO-SB2 and (b) ZnO-SU.

3.3.2. Effect of pH

The pH of the solution is critical for pollutant removal from wastewater. The influence of pH on MO removal using ZnO NPs was studied in batch experiments with a pH range of 1–7. The dye removal percentage versus the solution pH is presented in Figure 6(b). Figure 6(b) shows a steady increase in the MO percentage removals from pH 1.0 to 5.0 after which a slight decrease up to pH 7 was obtained. The maximum dye removal of 92% was observed with sample SB2 at the solution pH of 5.0. The decrease in dye removal after pH 5 is attributed to the interionic repulsion of negatively charged dye molecules and adsorbate surface. This result agrees with the study reported by Mokhtari *et al.* (2016), where the solution pH 5.0 showed the maximum MO removal by copper sulphide. The pH 4.0 was chosen for the following experiments due to its resemblance with real dye-polluted water.

3.3.3. The ZnO NP dose on MO removal

ZnO NP dose is essential to determine the synthesized ZnO NPs' capacity to remove a given concentration of MO. To investigate the effect of ZnO NP dose on MO removal, the adsorbent dose was varied from 0.01 to 0.05 g. Figure 6(c) shows the influence of sample dosage on the MO removal. MO removal percentage was observed to increase markedly with the increase of ZnO NP amount due to the increased adsorption sites in the lattice, and hence, the removal was enhanced. The maximum removal of MO was found to increase rapidly from 36 to 64% with increasing SB2 from 0.01 to 0.05 mg. The same trend was observed with other samples. The maximum removal for SB1 and SU was found to be 56 and 54%, respectively, using a 0.05 mg sample.

3.3.4. The dye concentration on MO removal

Figure 6(d) illustrates the relationship between the primary MO concentration and the dye removal percentage. The MO removal decreased with the increase in MO concentration. Increasing dye concentration from 5 to 20 mg/l decreased the dye removal from 67.9 to 25.7%, 52.0 to 28.8%, and 43 to 20% using SB2, SB1, and SU, respectively. The active sites of ZnO NPs get saturated beyond a particular concentration, which may decrease in dye removal with the increasing initial dye concentration. The same trend was reported by Suresh *et al.* (2015); Cai *et al.* (2016); and Silva *et al.* (2019).

To obtain isotherm information on the adsorption, the adsorption isotherm modelling of MO adsorption on the synthesized ZnO NPs was conducted. This was examined by three distinct isotherm models such as Langmuir, Freundlich, and Temkin models shown in Figure 7, and isotherm parameters are presented in Table 1. The

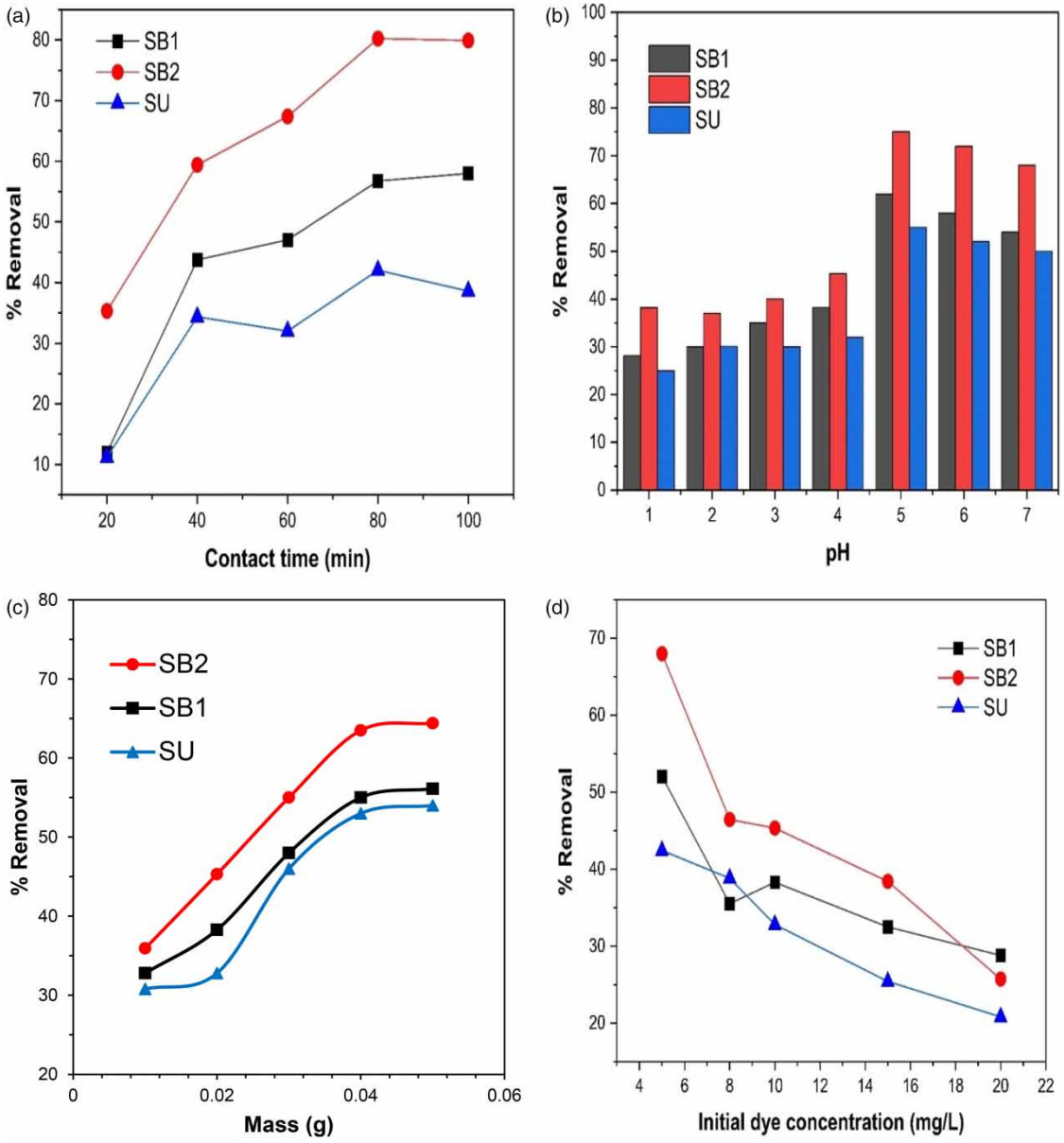

Figure 6 | The influence of (a) contact time, (b) pH of solution, (c) contact duration, and (d) primary MO concentration on dye uptake onto the synthesized ZnO NPs.

Langmuir, Freundlich, and Temkin isotherm equations are given as follows:

$$\text{Langmuir adsorption isotherm:} \quad \frac{C_e}{Q_e} = \frac{1}{K_l\, q_m} + \frac{C_e}{q_m}$$

$$\text{Freundlich adsorption isotherm:} \quad \ln Q_e = \ln K_F + \frac{1}{n}\ln C_e$$

$$\text{Temkin adsoprtion isotherm:} \quad Q_e = \frac{RT}{B}\ln K_T + \frac{RT}{B}\ln C_e$$

where Q_e, q_m, K_L, K_F, C_e, and K_T denote the equilibrium adsorption capacity (mg/g), Langmuir maximum monolayer adsorption capacity (mg/g), Langmuir constant, Freundlich constant, methyl orange dye concentration at equilibrium (mg/L), and the Temkin constant, respectively. B is the heat of adsorption (KJ/mol). The model constants are analysed from the slopes and intercepts of the model equations.

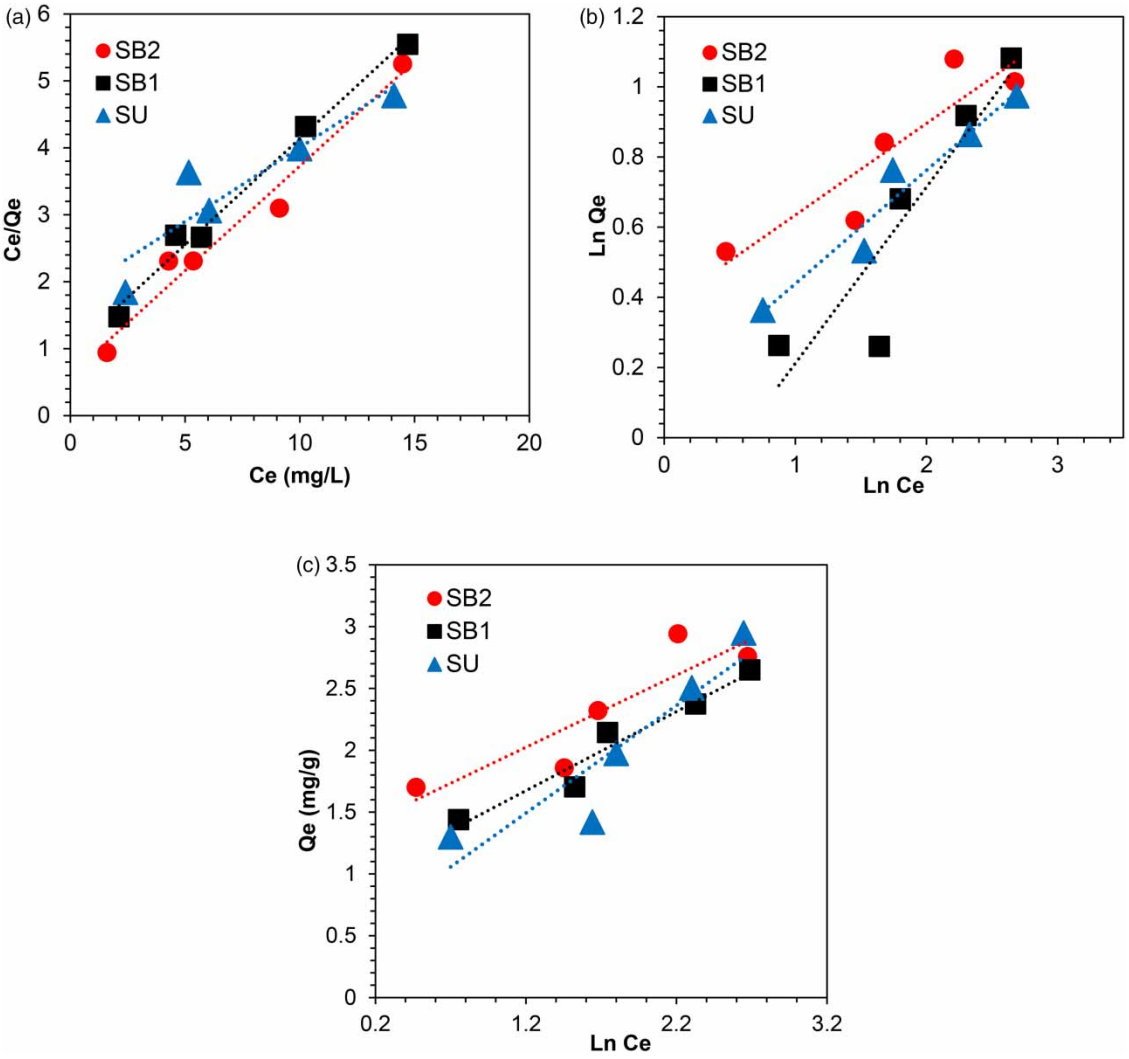

Figure 7 | (a) Langmuir, (b) Freundlich, and (c) Temkin isotherm plots for the methyl orange uptake by ZnO NPs.

The removal process of the used NPs fitted well with Langmuir. This isotherm revealed monolayer dye absorption on the adsorbent surface (Ezekoye *et al.* 2020). This result is consistent with the study reported by Zhang *et al.* (2016) and Zafar *et al.* (2019).

3.4. Zno NP synthesis and application from *S. persica*: comparison among other studies

Different studies investigated the green synthesis of ZnO and its application from *S. persica*. Table 2 summarizes a few of the reported studies with their synthesis and performance information.

It was obvious that the method of synthesis, synthesis agents, temperature condition, and extract source resulted in different outcomes including shape, size, and performance of ZnO NPs extracted from *S. persica*.

4. CONCLUSION

The study shows a green and promising synthesis process to synthesize ZnO NP with the use of *S. persica* leaf as a reducing and capping agent. The present study shows the effectiveness of the synthesized ZnO NPs for the removal of MO. The UV-Vis, EDX, and XRD showed a successful preparation of ZnO NPs. FTIR predicts the presence of phytochemicals for the effective formation of ZnO NPs. The SEM morphology presented a hexagonal and rod shape of ZnO NPs. The structural shape of ZnO NPs was highly influenced by the extract preparation method. The weight percentage of 58.2% Zn and 18.9% O_2 showed the maximum 80% MO removal at equilibrium removal. The MO removal was found to be influenced by various factors such as the shape of the synthesized ZnO NPs, contact time, initial concentration of dye, and solution pH. However, the shape of the synthesized ZnO NPs has a major influence on the removal of MO. The obtained results were analysed by the

Table 1 | The adsorption isotherm parameters for methyl orange uptake onto the synthesized ZnO NPs

	Langmuir isotherm		
	Constants		
ZnO NPs	KL (L/mg)	q_m (mg/g)	R^2
SB1	0.327	3.15	0.9872
SB2	0.517	3.2	0.9701
SU	0.221	4.51	0.871
	Freundlich isotherm		
	Constants		
ZnO NPs	N	K_f ((mg/g)(L/mg)$^{1/n}$))	R^2
SB1	3.091	1.122	0.9842
SB2	3.827	1.453	0.8265
SU	2.032	0.776	0.827
	Temkin isotherm		
	Constants		
ZnO NPs	B_t (J/mol)	K_t (L/mg)	R^2
SB1	0.6394	4.130	0.948
SB2	0.5827	9.735	0.8015
SU	0.8426	1.674	0.8429

Table 2 | Comparison between present study and other studies reporting ZnO NPs extracted from *S. persica*

Nanoparticles	*S. persica* extract	Extraction	Shape	Particle size	Weight %	Performance	Reference
ZnO	Root	Methanolic dispersion medium	NM	NM	Zn: 75.64% O_2: 24.36%	NS	Verma Khan & Banerjee (2020)
ZnO	Wood	Maceration method	Uniform hexagonal	60–130 nm	Zn: 67.46% O_2: 22.91%	Cytotoxic activity against cancer cell	Miri & Sarani (2019)
ZnO	Leaf	Using NaOH and $ZnCl_2$	Spherical honeycomb	30–50 nm	NS	95% removal of MB	Alharthi *et al.* (2020)
ZnO	Leaf	Using $Zn(NO_3)_2$. $6H_2O$ and heat	Hexagonal rod shaped	32–68 nm	Zn: 58.2% O_2: 18.9%	80% MO removal	This study

Note: NS: not studied; NM: not mentioned; MB: methylene blue; MO: methyl orange.

Langmuir, Freundlich, and Temkin isotherm models. The experimental data presented excellent fits for the isotherm models in the order: Langmuir > Freundlich > Temkin based on its correlation coefficient values. This study describes, for the first time, that different morphologies of ZnO can be obtained using the aqueous leaf extract of *S. persica*, and MO removal was found to be highly influenced by the structure of ZnO NPs.

DATA AVAILABILITY STATEMENT

All relevant data are included in the paper or its Supplementary Information.

CONFLICT OF INTEREST

The authors declare there is no conflict.

REFERENCES

Alamdari, S., Sasani Ghamsari, M., Lee, C., Han, W., Park, H.-H., Tafreshi, M. J., Afarideh, H. & Ara, M. H. M. 2020 Preparation and Characterization of Zinc Oxide Nanoparticles Using Leaf Extract of Sambucus Ebulus. *Applied Sciences (Switzerland)* **10**(10).

Alharthi, F. A., Alghamdi, A. A., Alothman, A. A., Almarhoon, Z. M., Alsulaiman, M. F. & Al-Zaqri, N. 2020 Green Synthesis of Zno Nanostructures Using Salvadora Persica Leaf Extract: Applications for Photocatalytic Degradation of Methylene Blue Dye. *Crystals* **10**(6).

Andres, M., Mifsud, A. & Serna, C. J. 1990 Formation of rod-like zinc oxide microcrystals in homogeneous solutions. *Journal of the Chemical Society, Faraday Transactions* **86**.

Aumeeruddy, M. Z., Zengin, G. & Mahomoodally, M. F. 2018 A review of the traditional and modern uses of *Salvadora persica* L. (Miswak): Toothbrush tree of prophet muhammad. *Journal of Ethnopharmacology* **213**, 409–444.

Basnet, P., Inakhunbi Chanu, T., Samanta, D. & Chatterjee, S. 2018 A review on bio-synthesized zinc oxide nanoparticles using plant extracts as reductants and stabilizing agents. *Journal of Photochemistry and Photobiology B: Biology* **183**, 201–221.

Cai, C. X., Xu, J., Deng, N. F., Dong, X. W., Tang, H., Liang, Y., Fan, X. & Li, Y. 2016 A Novel Approach of Utilization of the Fungal Conidia Biomass to Remove Heavy Metals from the Aqueous Solution through Immobilization. *Scientific Reports* 6.

Das, S., Das, J., Samadder, A., Bhattacharyya, S. S., Das, D. & Khuda-Bukhsh, A. R. 2013 Biosynthesized Silver Nanoparticles by Ethanolic Extracts of Phytolacca Decandra, Gelsemium Sempervirens, Hydrastis Canadensis and Thuja Occidentalis Induce Differential Cytotoxicity through G2/M Arrest in A375 Cells. *Colloids and Surfaces B: Biointerfaces* **101**, 325–36.

Ekennia, A. C., Uduagwu, D. N., Nwaji, N. N., Oje, O. O., Emma-Uba, C. O., Mgbii., S. I., Olowo, O. J. & Nwanji, O. L. 2021 Green Synthesis of Biogenic Zinc Oxide Nanoflower as Dual Agent for Photodegradation of an Organic Dye and Tyrosinase Inhibitor. *Journal of Inorganic and Organometallic Polymers and Materials* **31**(2), 886–97.

El-Rafie, H. M., El-Rafie, M. H. & Zahran, M. K. 2013 Green synthesis of silver nanoparticles using polysaccharides extracted from marine macro algae. *Carbohydrate Polymers* **96**(2), 403–410.

Ezekoye, O. M., Akomie, K. G., Chukwujindu, C. N. & Ujam, O. T. 2020 Biosorptive interaction of alkaline modified *Dialium guineense* seed powders with ciprofloxacin in contaminated solution: Central composite, kinetics, isotherm, thermodynamics, and desorption. *International Journal of Phytoremediation* **22**(10), 1028–1037.

Garg, N., Garg, A. & Mukherji, S. 2020 Eco-friendly decolorization and degradation of reactive yellow 145 textile dye by *Pseudomonas aeruginosa* and *Thiosphaera pantotropha*. *Journal of Environmental Management* **263**.

Gupta, A., Srivastava, P., Bahadur, L., Amalnerkar, D. P. & Chauhan, R. 2015 Comparison of Physical and Electrochemical Properties of ZnO Prepared via Different Surfactant-Assisted Precipitation Routes. *Applied Nanoscience (Switzerland)* **5**(7), 787–94.

Haque, M. M. & Alsareii, S. A. 2015 A review of the therapeutic effects of using miswak (*Salvadora persica*) on oral health. *Saudi Medical Journal* **36**(5), 530–543.

Iqbal, T., Raza, A., Zafar, M., Afsheen, S., Kebaili, I. & Alrobei, H. 2022 Plant-Mediated Green Synthesis of Zinc Oxide Nanoparticles for Novel Application to Enhance the Shelf Life of Tomatoes. *Applied Nanoscience (Switzerland)* **12**(2), 179–91.

Jan, H., Shah, M., Usman, H., Khan, M. A., Zia, M., Hano, C. & Abbasi, B. H. 2020 Biogenic Synthesis and Characterization of Antimicrobial and Antiparasitic Zinc Oxide (ZnO) Nanoparticles Using Aqueous Extracts of the Himalayan Columbine (Aquilegia Pubiflora). *Frontiers in Materials* **7**.

Joglekar, S., Kodam, K., Dhaygude, M. & Hudlikar, M. 2011 Novel route for rapid biosynthesis of lead nanoparticles using aqueous extract of *Jatropha curcas* L. latex. *Materials Letters* **65**(19–20), 3170–3172.

Kahsay, M. H., Tadesse, A., RamaDevi, D., Belachew, N. & Basavaiah, K. 2019 Green Synthesis of Zinc Oxide Nanostructures and Investigation of Their Photocatalytic and Bactericidal Applications. *RSC Advances* **9**(63), 36967–81.

Karnan, T. & Selvakumar, S. A. S. 2016 Biosynthesis of ZnO nanoparticles using rambutan (*Nephelium lappaceum* L.) peel extract and their photocatalytic activity on methyl orange dye. *Journal of Molecular Structure* **1125**, 358–365.

Khan, M.., Saadah, N. H., Khan, M. E., Harunsani, M. H., Tan, A. L. & Cho, M. H. 2019 Potentials of Costus Woodsonii Leaf Extract in Producing Narrow Band Gap ZnO Nanoparticles. *Materials Science in Semiconductor Processing* **91**, 194–200.

Khorsand Zak, A., Razali, R., Abd Majid, W. H. & Darroudi, M. 2011 Synthesis and characterization of a narrow size distribution of zinc oxide nanoparticles. *International Journal of Nanomedicine* **6**(1), 1399–1403.

Kowshik, M., Deshmukh, N., Vogel, W., Urban, J., Kulkarni, S. K. & Paknikar, K. M. 2002 Microbial Synthesis of Semiconductor CdS Nanoparticles, Their Characterization, and Their Use in the Fabrication of an Ideal Diode. *Biotechnology and Bioengineering* **78**(5), 583–88.

Lakshmeesha, T. R., Sateesh, M. K., Prasad, B. D., Sharma, S. C., Kavyashree, D., Chandrasekhar, M. & Nagabhushana, H. 2014 Reactivity of Crystalline ZnO Superstructures against Fungi and Bacterial Pathogens: Synthesized Using Nerium Oleander Leaf Extract. *Crystal Growth and Design* **14**(8), 4068–79.

Lengke, M. F., Fleet, M. E. & Southam, G. 2007 Biosynthesis of silver nanoparticles by filamentous Cyanobacteria from a silver(I) nitrate complex. *Langmuir* **23**(5), 2694–2699.

Matinise, N., Fuku, X. G., Kaviyarasu, K., Mayedwa, N. & Maaza, M. 2017 Zno nanoparticles via *Moringa oleifera* green synthesis: Physical properties & mechanism of formation. *Applied Surface Science* **406**, 339–347.

Mezohegyi, G., Zee, F. P., Font, J., Fortuny, A. & Fabregat, A. 2012 Towards Advanced Aqueous Dye Removal Processes: A Short Review on the Versatile Role of Activated Carbon. *Journal of Environmental Management* **102**, 148–64.

Miri, A. & Sarani, M. 2019 Biosynthesis and cytotoxic study of synthesized zinc oxide nanoparticles using *Salvadora persica*. *BioNanoScience* **9**(1), 164–171.

Modi, S., Yadav, V .K., Choudhary, N., Alswieleh, A. M., Sharma, A. K., Bhardwaj, A. K., Khan, S. H., Yadav, K. K., Cheon, J. K. & Jeon, B. H. 2022 Onion Peel Waste Mediated-Green Synthesis of Zinc Oxide Nanoparticles and Their Phytotoxicity on Mung Bean and Wheat Plant Growth. *Materials* **15**(7), 2393.

Mokhtari, P., Ghaedi, M., Dashtian, K., Rahimi, M. R. & Purkait, M. K. 2016 Removal of Methyl Orange by Copper Sulfide Nanoparticles Loaded Activated Carbon: Kinetic and Isotherm Investigation. *Journal of Molecular Liquids* **219**, 299–305.

Nava, O. J., Soto-Robles, C. A., Gómez-Gutiérrez, C. M., Vilchis-Nestor, A. R., Castro-Beltrán, A., Olivas, A. & Luque, P. A. 2017 Fruit Peel Extract Mediated Green Synthesis of Zinc Oxide Nanoparticles. *Journal of Molecular Structure* **1147**, 1–6.

Pacholski, C., Kornowski, A. & Weller, H. 2002 Self-assembly of ZnO: From nanodots to nanorods. *Angewandte Chemie International Edition* **41**. Available from: www.ccdc.cam.ac.uk/conts/.

Pathania, D., Kumar, S., Thakur, P., Chaudhary, V., Kaushik, A., Varma, R. S., Furukawa, H., Sharma, M. & khosla, A. 2022 Essential Oil-Mediated Biocompatible Magnesium Nanoparticles with Enhanced Antibacterial, Antifungal, and Photocatalytic Efficacies. *Scientific Reports* **12**(1).

Patil, B. N. & Taranath, T. C. 2018 *Limonia acidissima* L. leaf mediated synthesis of silver and zinc oxide nanoparticles and their antibacterial activities. *Microbial Pathogenesis* **115**, 227–232.

Peerakiatkhajohn, P., Butburee, T., Sul, J.-H., Thaweesak, S. & Yun, J.-H. 2021 Efficient and rapid photocatalytic degradation of methyl orange dye using Al/ZnO nanoparticles. *Nanomaterials* **11**(4), 1059.

Rautaray, D., Ahmad, A. & Sastry, M. 2003 Biosynthesis of $CaCO_3$ crystals of complex morphology using a fungus and an actinomycete. *Journal of the American Chemical Society* **125**(48), 14656–14657.

Reuben, D. K., Aji, S., Andrew, W. & Inna, F. 2011 Preliminary phytochemical screening and in vitro anthelmintic effects of aqueous extracts of *Salvadora persica* and *Terminalia avicennoids* against strongyline nematodes of small ruminants in Nigeria. *Journal of Animal and Veterinary Advances* **10**(4), 437–442.

Salahuddin, N. A., El-Kemary, M. & Ibrahim, E. M. 2015 Synthesis and characterization of ZnO nanoparticles via precipitation method: Effect of annealing temperature on particle size. *Nanoscience and Nanotechnology* **5**(4), 82–88.

Selim, Y. A., Azb, M. A., Ragab, I. & Abd El-Azim, M. H. M. 2020 Green synthesis of zinc oxide nanoparticles using aqueous extract of Deverra tortuosa and their cytotoxic activities. *Scientific Reports* **10**(1), 3445.

Sendal, K., Ustün Ozgur, M. & Gulen, J. 2022 Biosynthesis of ZnO photocatalyst and its application in photo catalytic degradation of methylene blue dyestuff. *Journal of Dispersion Science and Technology* **44**(14), 2734–2747.

Sharma, S. C. 2016 Zno nano-Flowers from *Carica papaya* milk: Degradation of alizarin Red-S dye and antibacterial activity against *Pseudomonas aeruginosa* and *Staphylococcus aureus*. *Optik* **127**(16), 6498–6512.

Sharma, P., Urfan, M., Anand, R., Sangral, M., Hakla, H. R., Shubham, S., Das, R., Pal, S. & Bhagat, M. 2022 Green Synthesis of Zinc Oxide Nanoparticles Using Eucalyptus Lanceolata Leaf Litter: Characterization, Antimicrobial and Agricultural Efficacy in Maize. *Physiology and Molecular Biology of Plants* **28**(2), 363–81.

Silva, F., Nascimento, L., Brito, M., da Silva, K., Paschoal, W. & Fujiyama, R. 2019 Biosorption of Methylene Blue Dye Using Natural Biosorbents Made from Weeds. *Materials* **12**(15), 2486.

Suresh, D., Nethravathi, P. C., Udayabhanu., Rajanaika, H., Nagabhushana, H. & Sharma, S. C. 2015 Green Synthesis of Multifunctional Zinc Oxide (ZnO) Nanoparticles Using Cassia Fistula Plant Extract and Their Photodegradative, Antioxidant and Antibacterial Activities. *Materials Science in Semiconductor Processing* **31**, 446–54.

Suresh, J., Pradheesh, G., Alexramani, V., Mahalingam Sundrarajan, M. & Hong, S. 2018 Green Synthesis and Characterization of Zinc Oxide Nanoparticle Using Insulin Plant (Costus Pictus D. Don) and Investigation of Its Antimicrobial as Well as Anticancer Activities. *Advances in Natural Sciences: Nanoscience and Nanotechnology* **9**(1), 015008.

Vargas, M., Eric, M., Rivera-Muñoz, E., Diosa, J., Mosquera, E. & Rodríguez-Páez, E. J. 2021 Nanoparticles of ZnO and Mg-Doped ZnO: Synthesis, Characterization and Efficient Removal of Methyl Orange (MO) from Aqueous Solution. *Ceramics International* **47**(11), 15668–81.

Verma, P. R., Khan, F. & Banerjee, S. 2020 *Salvadora persica* root extract-mediated fabrication of ZnO nanoparticles and characterization. *Inorganic and Nano-Metal Chemistry* **51**(3), 1–7.

Xu, J., Huang, Y., Zhu, S. & Abbes, N. 2021 A review of the green synthesis of ZnO nanoparticles using plant extracts and their prospects for application in antibacterial textiles. *Journal of Engineered Fibers and Fabrics* **16**, 1–14.

Yang, S. J. & Park, C. R. 2008 Facile preparation of monodisperse ZnO quantum dots with high quality photoluminescence characteristics. *Nanotechnology* **19**(3), 035609.

Yedurkar, S., Maurya, C. & Mahanwar, P. 2016 Biosynthesis of zinc oxide nanoparticles using *Ixora coccinea* leaf extract – A green approach. *Open Journal of Synthesis Theory and Applications* **05**(01), 1–14.

Zafar, M. N. Dar, Q., Nawaz, F., Zafar, M. N., Iqbal, M. & Nazar, M. F. 2019 Effective adsorptive removal of Azo dyes over spherical ZnO nanoparticles. *Journal of Materials Research and Technology* **8**(1), 713–725.

Zhang, F., Chen, X., Wu, F. & Ji, Y. 2016 High adsorption capability and selectivity of ZnO nanoparticles for dye removal. *Colloids and Surfaces A: Physicochemical and Engineering Aspects* **509**, 474–483.

First received 21 October 2023; accepted in revised form 8 February 2024. Available online 27 February 2024